Journal of Alloys and Compounds 722 (2017) 474–481

Contents lists available at ScienceDirect

Journal of Alloys and Compounds

journal homepage: http://www.elsevier.com/locate/jalcom

Preparation of single-phase SnSe thin-films and modification of electrical properties via stoichiometry control for photovoltaic application

Giuk Jeong [a], Jekyung Kim [a], Oki Gunawan [b], Seong Ryul Pae [a], Soo Hyun Kim [c], Jae Yong Song [d, ***], Yun Seog Lee [b, **], Byungha Shin [a, *]

[a] Dept. of Materials Science and Engineering, Korea Advanced Institute of Science and Technology, 291 Daehak-ro, Yuseong-gu, Daejeon, 34141, Republic of Korea
[b] IBM T. J. Watson Research Center, Yorktown Heights, NY 10598, USA
[c] Dept. of Materials Science and Engineering, Yeungnam University, 280, Daehak-ro, Gyeongsan-si, Gyeongsangbuk-do, 38541, Republic of Korea
[d] Korea Research Institute of Standards and Science, 267 Gajeong-ro, Yuseong-gu, Daejeon, 34113, Republic of Korea

ARTICLE INFO

Article history:
Received 11 March 2017
Received in revised form
5 June 2017
Accepted 8 June 2017
Available online 12 June 2017

Keywords:
Thin films
Inorganic materials
Electronic properties
Electronic band structure
Photoconductivity and photovoltaics

ABSTRACT

Single-phase SnSe thin films were prepared via thermal co-evaporation using a Se thermal cracker. By carefully tuning the stoichiometry of the SnSe, we found that the composition range of single phase SnSe is very narrow, a Se/Sn ratio of 0.95–0.99; outside of this range secondary phases (metallic Sn or $SnSe_2$) formed. Electrical properties were found to be very sensitive to even small changes in the stoichiometry. Three orders of magnitude difference in the carrier concentration was observed within the stoichiometry range for single-phase SnSe, which can be explained by changes in the shallow level defect density. To further control carrier concentration, we introduced In and Sb as counter-dopants into the SnSe thin films and found that they were deep level donors with the ionization fraction of ~10^{-4}. Finally, we demonstrate the potential of SnSe thin films as an absorber layer in photovoltaic applications. Our study demonstrates the importance of fine-tuning stoichiometry of SnSe to achieve desired electrical properties.

1. Introduction

Metal chalcogenide (e.g. SnS, SnSe, Sb_2S_3) thin-films have been considered as a novel class of materials for photovoltaic applications with a terawatt-level scalability, due to their tunable bandgaps and earth-abundant elemental constituents [1–3]. Photovoltaic devices based on SnS and Sb_2Se_3 have been investigated using various film deposition techniques, such as thermal evaporation [4], atomic layer deposition [5], chemical bath deposition [6], and sputtering [7]. The highest power conversion efficiency of photovoltaic device based on these films have been 7.5% and 4.36% for Sb_2S_3 [8] and SnS [1], respectively. In the case of SnSe, however, studies have been made for thermoelectric applications because of its intrinsically low thermal conductivity. Zhao et al. reported the ZT value of 2.62 which was the highest ZT value reported among all thermoelectric materials [9]. After this report, numerous research efforts on thermoelectric study of SnSe have followed. Shafique et al. [10] and Xiao et al. [11] calculated fundamental thermoelectric properties of binary 2D chalcogenides. Recently, Zhao et al. reported a high ZT of 1.34 via Na doping [12]. More recently, Duong, et al. reported the Bi-doped n-type SnSe single crystals with ZT factor of 2.2 [13]. However, photovoltaic applications based on SnSe thin-films have not been reported, largely due to the difficulty in synthesizing single-phase SnSe thin-films. Secondary phases (e.g. metallic Sn, $SnSe_2$, and Sn_2Se_3) in the SnSe absorber layer in solar cells often increase the density of non-radiative recombination centers, resulting in a limited power conversion efficiencies in the devices [14]. The Sn–Se system is known to have a very narrow composition range for a pure SnSe [15], which requires precisely controlled processes for the film preparation.

In this paper, we report on the fabrication of single-phase SnSe thin-films by thermal co-evaporation with a thermal cracking

* Corresponding author.
** Corresponding author.
*** Corresponding author.
E-mail addresses: jysong@kriss.re.kr (J.Y. Song), yslee@us.ibm.com (Y.S. Lee), byungha@kaist.ac.kr (B. Shin).

http://dx.doi.org/10.1016/j.jallcom.2017.06.094
0925-8388/

source for selenium and post-annealing. There have been some reports about fabrication of SnSe thin films via thermal evaporation method [3,16,17]. However, thermal co-evaporation with a Se thermal cracker has not been reported. The compositions of the films are precisely tuned with the fluxes of Se and Sn vapor by controlling the temperature of each effusion cell. The evaporated films were then annealed in a furnace with N_2 atmosphere. We investigate the composition window for a single-phase SnSe thin-film deposition. The electrical properties of the films were studied by varying the composition ratio of Se and Sn. Dramatic changes in electrical properties, in particular alteration of carrier density from ~10^{16} to ~10^{18} cm^{-3}, were observed in a narrow range the Se/Sn ratio between 0.9 and 1.1. The significant increase in carrier density can be explained by the change in the relative population of the Sn-vacancy, as suggested by theoretical calculations [18]. Furthermore, we investigate extrinsic doping with In and Sb to reduce the carrier density that is more suitable for photovoltaic application. A working SnSe photovoltaic device is also demonstrated.

2. Experimental

2.1. SnSe thin-film preparation

1–2 μm thick SnSe films were deposited on borosilicate glass substrates by thermal co-evaporation method. The substrate was heated to ~100 °C and the pressure of chamber was kept below 1×10^{-6} Torr. The Sn- and Se-flux were controlled by adjusting the temperature of a Sn effusion cell and the reservoir of a Se thermal cracker. A thermal cracker kept at 800 °C was used to generate highly reactive Se molecules (*e.g.* Se and Se_2) from large Se molecules (*e.g.* Se_8 and Se_4). By using the cracked Se source, we were able to reduce the substrate temperature for growing high-quality SnSe thin-films [18,19]. After the film deposition, the SnSe films were annealed at 500 °C, 5 min by using a hot plate in a N_2-filled glove box [20,21]. In and Sb dopants were introduced by thermal diffusion. 10-nm-thick doping layers (Sb_2Se_3 or In thin films) were deposited either on borosilicate glass substrates prior to the SnSe deposition process (in the case of the Sb_2Se_3) or on top of the SnSe films (in the case of the In). The bi-layer samples (Sb_2Se_3/SnSe and SnSe/In) were then annealed for 5 min at 500 °C to prepare Sb- and In-doped SnSe thin-film samples, as schematically shown in Fig. 1.

2.2. Characterization and measurements

Morphology of SnSe thin-films were investigated using scanning electron microscopy (SEM). Samples were coated with a thin Pt layer by sputtering. Composition of the films were measured by energy-dispersive X-ray spectroscopy (EDS) and inductively coupled plasma atomic emission spectroscopy (ICP). The crystalline structure was investigated by X-ray diffraction (XRD) with a Cu-Kα radiation source (RIGAKU Ultima IV). Raman spectroscopy (ARAMIS, Horiba Jobin Yvon) was used to detect secondary phases that may exist below the XRD detection limit. An Ar-ion CW laser (514 nm) was used for the Raman measurement in the range of 100 cm^{-1}–500 cm^{-1}. To investigate the optical properties of the films, UV-VIS-NIR spectrometer (Lambda 1050) was used in the range of 190–3300 nm. In ultraviolet photoelectron spectroscopy (UPS) (Sigma Probe), a He-I excitation (21.2 eV) and 10 V acceleration voltage were used to measure the Fermi level and valance band position of the films. Electrical properties of the films were measured by Hall effect measurement in which 1 μA current and ±0.7 T magnetic field were used.

3. Results

3.1. Preparation of single phase SnSe thin films

Single-phase SnSe thin-films were fabricated by thermal co-evaporation and post-annealing processes. The flux of Se and Sn were controlled by varying the temperature of each effusion cell. Then the samples were annealed at 500 °C under nitrogen ambient without additional Se over-pressure. Conventional photovoltaic chalcogenide compounds such as $Cu_2ZnSn(S,Se)_4$ (CZTS) and Cu(In, Ga)$(S,Se)_2$ (CIGS) require additional S or Se sources for annealing to prevent the film decomposition induced by S or Se sublimation [21–23]. For SnSe, however, we observed that Se over-pressure during annealing induced the emergence of $SnSe_2$ phase. Therefore, we did not applied the Se over-pressure during annealing. By adjusting the relative ratio of Sn and Se flux during evaporation, we can modify the morphology of the film as shown in Fig. 2.

In Fig. 2, from (a,e) to (d,h), the Se/Sn ratio reduces. Changes in the Se/Sn ratio led to dramatic changes in morphology from (a, e) to (d, h). We observed that densely packed grain were shown in (c,g) and (d,h) while plate-like grains were shown in (a,e), (b,f). The grain size of the (c, g) film is ~1 μm, which is the largest grain size among the samples. For a photovoltaic absorber layer large grain size is advantageous to minimize non-radiative recombination of photo-generated carriers at grain boundaries. In (a, e), the film consists of only the $SnSe_2$ phase. From Fig. 2(a, e), we increased the Sn flux to fabricate the SnSe film. Fig. 2(b, f) is a mixture of SnSe and $SnSe_2$ and eventually Fig. 2(c, g) consists of only SnSe phase. When Sn flux was further increased, elemental Sn precipitated inside the SnSe thin films Fig. 2(d, h). The lattice structure of each samples was measured by XRD as shown in Fig. 3.

In Fig. 3a, b, c and d correspond to (a,e), (b,f), (c,g), (d,h) in Fig. 2. Each XRD peak was identified by JCPDS No. 48-1224 (*Pnma* SnSe), 23-0602 ($P\bar{3}m1$ $SnSe_2$), and 04-0673 (elemental Sn). In Fig. 3(c), all XRD peaks are accounted by *Pnma* SnSe phase. However, it is possible that secondary phases may exist below the XRD detection limit (~2 wt% of sample). Raman spectroscopy, which has lower detection limit (~ppm), was therefore carried out.

In Fig. 4(b), we observed that $SnSe_2$ and Sn_3O_4 co-exist in the film. Sn_3O_4 peaks were detected on 140 cm^{-1} and 170 cm^{-1} [24]. Because Fig. 4(b) was Sn-rich, excess Sn on the surface combined with oxygen in the air and tin oxide was produced on the film

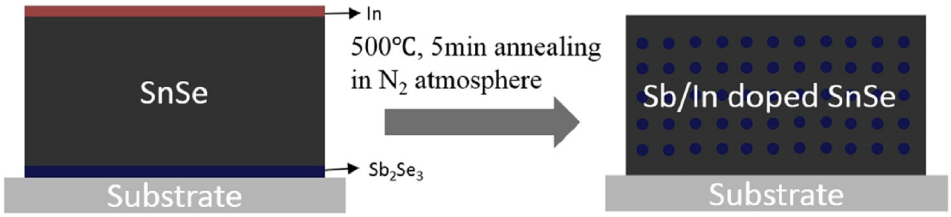

Fig. 1. Schematic of doping mechanism.

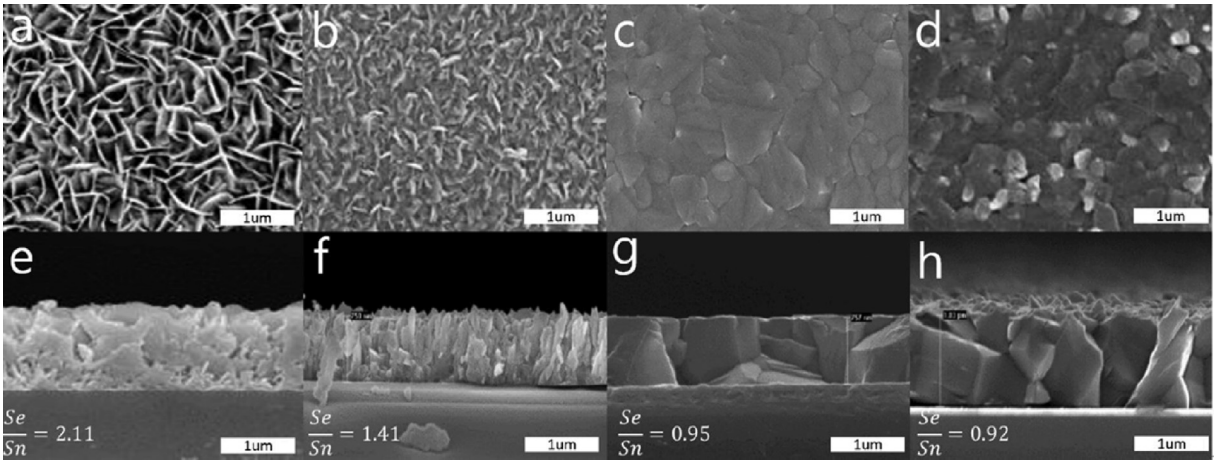

Fig. 2. Cross-section SEM image of prepared SnSe thin-films. Sn and Se compound as composition changes. (a, e) − $SnSe_2$ (b, f) SnSe + $SnSe_2$, (c, g) − SnSe, (d, h) Sn + SnSe.

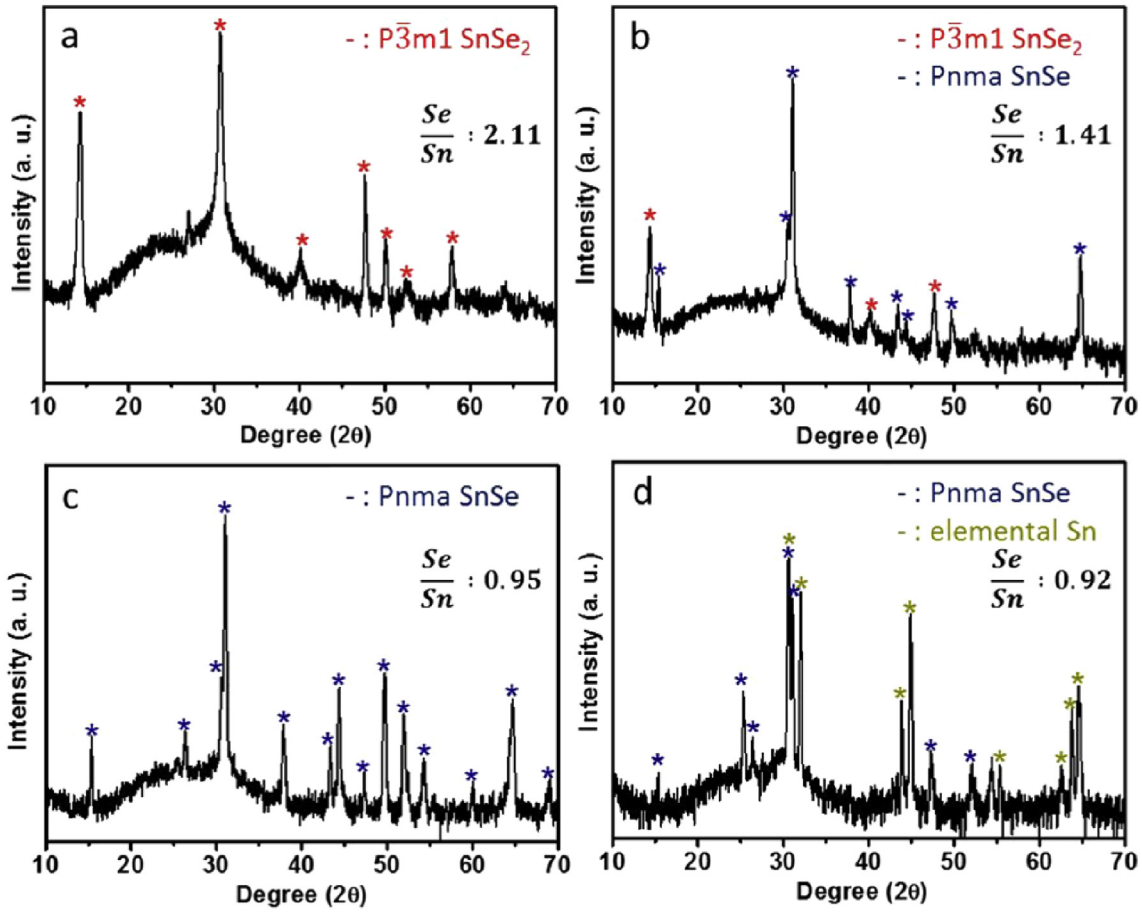

Fig. 3. XRD θ-2θ scans of Sn and Se compound with varying stoichiometry.

surface. In Fig. 4(a), only SnSe Raman peaks are detected on 108 cm^{-1} (B_{3g} vibration mode), 128 cm^{-1} and 150 cm^{-1}(A_g vibration mode) [25,26]. So, we concluded that pure phase SnSe thin film was fabricated as analyzed by SEM, XRD and Raman spectroscopy. We then tried to figure out the electrical and optical properties of single phase SnSe thin film. UV–vis spectroscopy, UPS and Hall measurement were used as analyzing tools. Note that the SnSe thin films used for optical and electrical characterization has Se/Sn ratio of 0.99, slightly higher Se/Sn ratio that the one used for structural characterizations, which is still a pure phase SnSe. Band structure and optical properties of film is shown in Fig. 5.

Based on the absorbance values obtained from UV–vis spectroscopy, the absorption coefficient (α) is calculated by the relation below:

$$\alpha = 2.303(A/t), \tag{1}$$

where A and t are the absorbance and the film thickness,

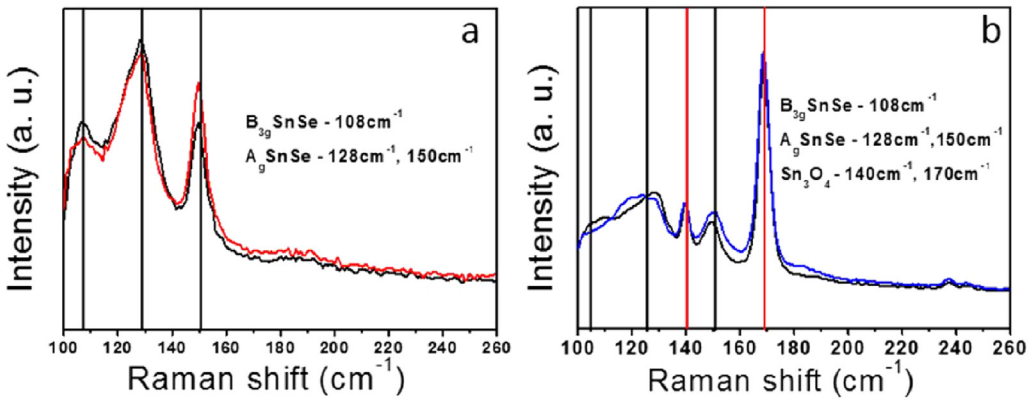

Fig. 4. Raman spectra of (a) pure SnSe sample (Fig. 3(c)) and (b) Sn rich SnSe sample (Fig. 3(d)). 514 nm laser was used for the measurement.

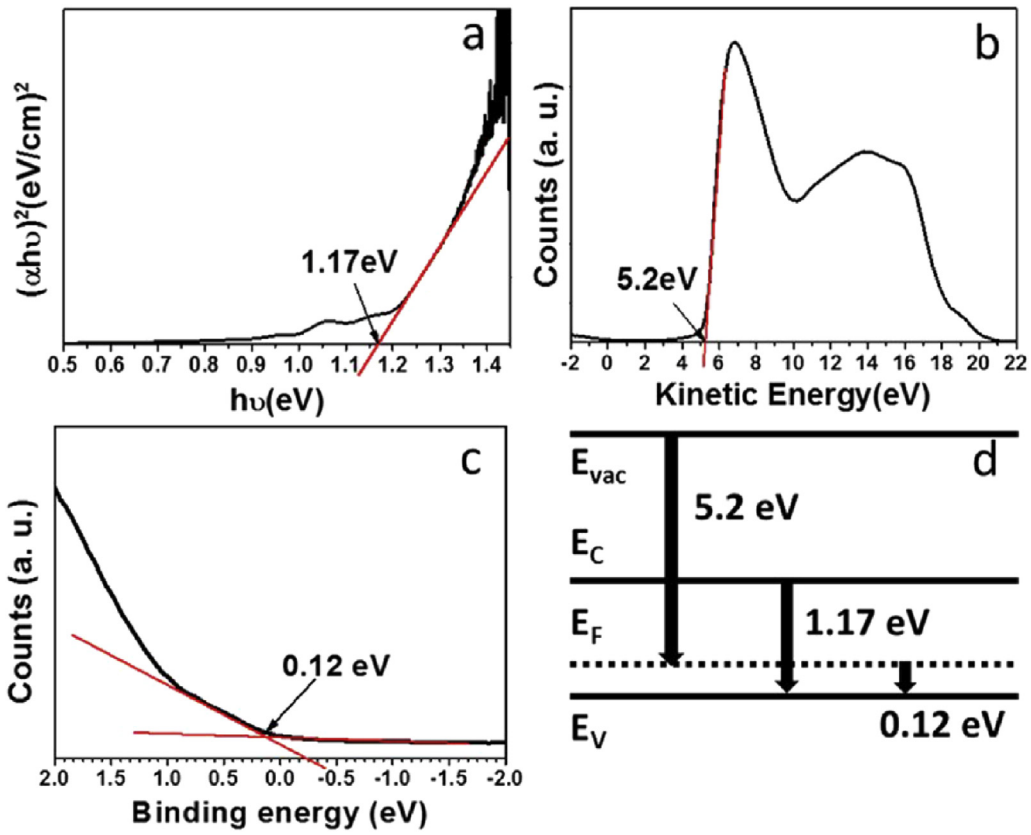

Fig. 5. Optical properties of single phase SnSe thin films. (a) Tauc plot from UV-VIS-NIR spectroscopy (b, c) the first cutoff (b) and secondary cutoff (c) of UPS of SnSe thin films (d) Estimated band structure of SnSe thin-films.

respectively. From 400 to 900 nm, the absorption coefficient of SnSe film was around 8×10^4 cm^{-1}, comparable to other good photovoltaic absorber materials [27,28]. By using a Tauc plot shown in Fig. 5(a), the direct band gap of the film was estimated to be ~1.17 eV, which is 0.2 eV larger than DFT calculated value [29]. This estimated values obtained from Tauc plot was well matched with previous results, which are 1.1 eV, 1.19 eV, 1.21 eV, respectively [30–32]. UPS was measured to estimate the valence band maximum (VBM) of SnSe thin film. In Fig. 5(b and c), extrapolation of first and secondary offsets reveals that the SnSe thin film has a work function of 5.2 eV and a Fermi-level at 0.12 eV above the VBM. Fig. 5(d) depicts the estimated band structure of the SnSe thin-films, suggesting a p-type conductivity. The electrical properties of the film is also measured by Hall effect measurements, which revealed that the SnSe thin film has a carrier concentration of 1.03×10^{17} cm^{-3}, mobility of 1.27 cm^2/V·s, resistivity of 48.2 Ω cm, and Hall coefficient of 61.0 cm^3/C. With these measurements, hole effective mass of the SnSe thin-film is estimated to be 5.16×10^{-31} *kg* ($0.56m_0$) by the following relations [33]:

$$p = N_v \exp\{(E_v - E_F)/kT\}, \tag{2}$$

$$m^* = (N_v/2)^{2/3} h^2 \Big/ 2\pi kT, \tag{3}$$

where N_v, E_v, E_F, k, and T are effective valence band density of state,

valence band maximum, Fermi level, Boltzmann constant, and temperature, respectively. All the quantities except N_v are known, therefore, m^* is determined. The calculated hole effective mass is consistent with the literature value due to Zhao, et al. [13] and Shi, et al. [34].

The Hall measurement indicates that SnSe thin films exhibit p-type conductivity and high carrier concentration in the order of 10^{17}, which is consistent with the calculated values from the position of E_F with respect to the valence band maximum. The current values of carrier concentration and resistivity are inappropriate for an absorber layer in photovoltaic applications; the ideal carrier concentration for solar absorbers is in the range of 10^{14}–10^{16} cm^{-3} [19,35]. To identify the optimal carrier density of SnSe thin-films as a light absorber, we calculated the carrier density-dependent depletion width of SnSe films. Depletion width is calculated by the relation below [30]:

$$x_d = x_n + x_p = \sqrt{\frac{2\varepsilon_{s,n}\varepsilon_{s,p}}{q}\frac{(N_A+N_D)^2(V_{bi}-V_a)}{N_A N_D\left(N_A\varepsilon_{s,p}+N_D\varepsilon_{s,n}\right)}}, \quad (4)$$

where $\varepsilon_{s,n}$, $\varepsilon_{s,p}$, N_A, N_D, V_{bi}, and V_a are permittivity of n-type and p-type layers, density of ionized acceptors and donors, built-in voltage, and applied bias, respectively. By assuming $N_D \gg N_A$, which is reasonable for SnSe/CdS heterojunction (CdS is the most commonly used buffer layer for chalcogenide thin film solar cells), the relation is simplified to

$$x_d = x_n + x_p \approx x_p \approx \sqrt{\frac{2\varepsilon_{s,p}}{q}\frac{(V_{bi}-V_a)}{N_A}}, \quad (5)$$

where V_{bi} and $\varepsilon_{s,p}$ are 0.7 V and $9.94\varepsilon_0$ [36], respectively. For N_A of 10^{15}–10^{17} cm^{-3}, depletion width inside the SnSe is estimated to be ~877 nm ($N_A = 10^{15}$ cm^{-3}) and ~87 nm ($N_A = 10^{17}$ cm^{-3}). Because too narrow a depletion width inside a light absorbing layer is disadvantageous for charge collection, we conclude that carrier density of SnSe thin-films should be reduced to the order of 10^{15} cm^{-3}. In order to reduce the carrier concentration, we modified the electrical properties by stoichiometric control and by introducing foreign dopant elements into the films.

3.2. Stoichiometric control of SnSe thin films and its effect on electrical properties

The stoichiometry of the SnSe thin-films was adjusted between Se/Sn values of 0.9–1.1 by controlling Sn and Se flux during co-evaporation. As shown in Table 1, a small variation in the stoichiometry, especially between the Se/Sn ratio of 0.95 and 1.01, resulted in remarkable change in electrical properties.

The results show that Se-rich SnSe (Se/Sn > 1) has a more resistive characteristic and Sn-rich SnSe (Se/Sn < 1) has a more conductive characteristic than the pristine SnSe thin films. The dramatic change in the carrier concentration can be explained by the expected density of Sn vacancy. Theoretical calculations [37,38] suggest that p-type conductivity of SnSe originates from Sn vacancies. In tin (Sn)-chalcogenide (X = S or Se) system, there are six types of native point defects—vacancy (V_{Sn}, V_X), interstitials (Sn_i, X_i), and antisite defects (Sn_X, X_{Sn}). In the case of SnS, DFT calculation showed that the V_{Sn} has the lowest formation energy when the sample is S-rich. Also, the transition level of V_{Sn} is close to the valance band edge, which means that V_{Sn} acts as a shallow level acceptor. In case of Sn-rich sample, V_S and Sn_s have lower defect formation energy than V_{Sn}. However, the transition levels of those defects are close to the Fermi level, which means that they are deep level defects and do not make a significant contribution to the conductivity of the sample. Given the chemical similarity between SnS and SnSe, it is anticipated that the major acceptor in SnSe thin-films is also V_{Sn}, and the carrier density is predominantly determined by the concentration of Sn vacancies. In the case of Sn-rich samples, the population of V_{Sn} is expected to decrease compared to a pristine SnSe while it is opposite for Se-rich samples. As shown in Fig. 6, in XRD measurements of samples within a narrow range of the Se/Sn ratio between 0.95 and 0.99, all the peaks can be assigned to SnSe. Outside of this range, $SnSe_2$ (Se/Sn > 0.99) or elemental Sn (Se/Sn < 0.95) is found. If secondary phases affect electrical properties of film, the Se-rich SnSe should be more resistive because of the n-type nature of $SnSe_2$ that would counteract the p-type conductivity of the SnSe host and the Sn-rich SnSe should be more conductive due to the inclusion of metallic Sn phase. This is opposite to our observation suggesting that the effect of secondary phase on electrical conductivity is negligible.

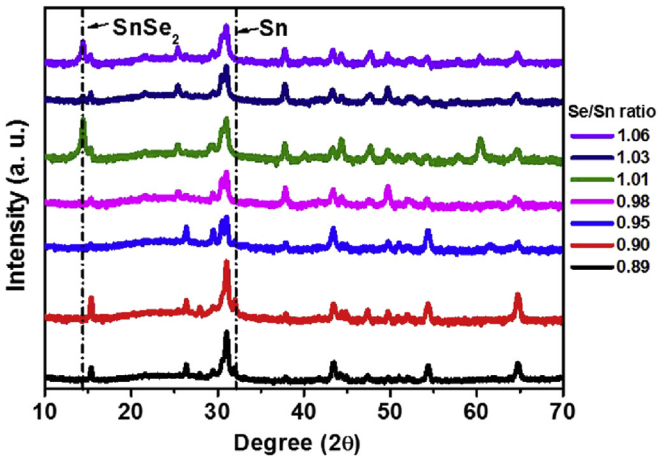

Fig. 6. XRD graph of SnSe thin films with different Se/Sn ratio. All the peaks without two peaks indicated above are *Pnma* SnSe peaks.

Table 1
Electrical Properties of SnSe thin films as function of the Se/Sn ratio. Values inside the parenthesis are an error bar of measured values.

Se/Sn ratio	Carrier density (/cm^3)	Mobility (cm^2/V·s)	Resistivity (Ω·cm)	Conductivity (S/cm)
0.89	$1.35\times10^{15}(\pm0.30)$	$2.98\times10^{1}(\pm0.55)$	$1.60\times10^{2}(\pm0.46)$	$7.17\times10^{-3}(\pm0.46)$
0.90	$2.92\times10^{15}(\pm0.27)$	$1.07\times10^{1}(\pm0.37)$	$2.12\times10^{2}(\pm0.09)$	$4.74\times10^{-3}(\pm0.09)$
0.95	$2.98\times10^{15}(\pm0.11)$	$7.96\times10^{0}(\pm0.09)$	$2.64\times10^{2}(\pm0.08)$	$3.80\times10^{-3}(\pm0.08)$
0.98	$2.83\times10^{16}(\pm0.27)$	$5.81\times10^{1}(\pm0.26)$	$3.90\times10^{0}(\pm0.04)$	$2.57\times10^{-1}(\pm0.04)$
1.01	$7.49\times10^{17}(\pm0.16)$	$5.77\times10^{0}(\pm0.18)$	$1.47\times10^{0}(\pm0.01)$	$6.85\times10^{-1}(\pm0.01)$
1.03	$1.36\times10^{18}(\pm0.29)$	$4.06\times10^{0}(\pm0.62)$	$1.64\times10^{0}(\pm0.04)$	$6.11\times10^{-1}(\pm0.04)$
1.06	$7.66\times10^{17}(\pm0.40)$	$6.59\times10^{0}(\pm0.76)$	$1.57\times10^{0}(\pm0.05)$	$6.39\times10^{-1}(\pm0.05)$

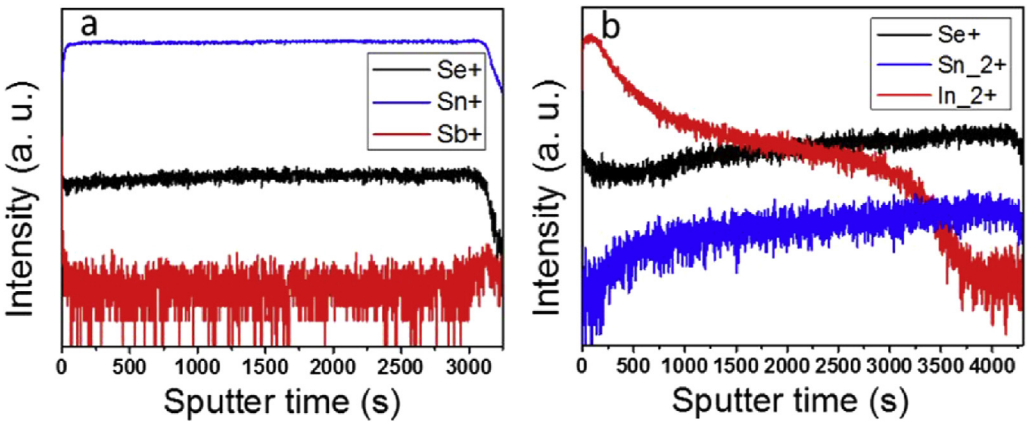

Fig. 7. SIMS depth profile of Sb doped SnSe(a) and In doped SnSe(b).

3.3. Introducing counter dopants to SnSe thin films

To further reduce the carrier concentration of the SnSe thin films, extrinsic counter dopants (donors) such as Sb and In were introduced to SnSe thin films. Sinsermsuksakul, et al. reported the reduction of electrical conductivity of SnS thin films via doping with Sb [39]. We introduced Sb (or In) to SnSe by thermal evaporation of Sb_2Se_3 (or In) followed by thermal-induced diffusion process. SIMS depth-profile of the Sb- and In-doped samples were measured to investigate the distribution profiles of each dopant in the films (Fig. 7).

The SIMS results show that both Sb and In were well diffused into the entire depth of the SnSe films. In case of the In-doped SnSe, we deduce that the post-annealing time was not sufficiently long to ensure a uniform distribution of In inside the SnSe. Hall measurements performed on the In- and Sb-doped SnSe films showed an obvious decrease in the carrier density and electrical conductivity compared to the undoped sample (Table 2). When the impurities were diffused into the film, there are possibilities of substitutional or interstitial occupation, or precipitation inside the film. Given similar ionic radii of Sn and Sb (or In), it is expected that the interstitial occupation of Sb (or In) would be a rare event. From the XRD results from the Sb- and In-doped samples, no secondary phase or metallic phase of the dopants were observed (Fig. 8). Therefore we expected that the majority of the dopants inside the SnSe films occupied substitutional sites, acting as counter dopants and reducing the hole density. If all the Sb or In dopants are located at Sn substitutional site, the fraction of the ionized donors is determined by comparing the total concentration of the impurities introduced (which is estimated from the thickness of the deposited impurity layer) and the value of the reduction in hole concentration via the doping. The ionization fraction is on the order of 10^{-4}. From this small ratio of the dopant activation, we conclude that Sb and In in SnSe are deep level donors. It is interesting to note that this extrinsic doping approach was only successful in single phase SnSe films; in the case of Se- and Sn-rich SnSe films, neither Sb nor In worked as counter dopants. Further work is needed to understand this composition-dependence of extrinsic doping behavior.

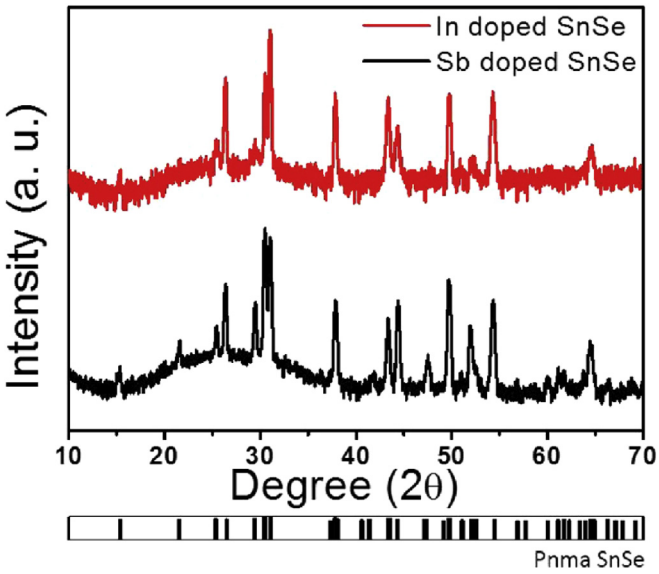

Fig. 8. XRD spectra of In/Sb-doped SnSe. All the peaks are identified as *Pnma* SnSe.

Fig. 9 presents the summary of the correlation between carrier concentration and stoichiometry as well as the effects of the extrinsic doping. It should be noted that the range of Se/Sn ratio where single phase SnSe are fabricated is very narrow. And even in this range, carrier density of the SnSe thin films changes dramatically. Considering the carrier density, SnSe thin films between Se/Sn ratio 0.96 and 0.97 are found to be suitable for photovoltaic application. We fabricated photovoltaic devices with a structure shown in Fig. 10. Device shows rectified I-V characteristic with 0.2% power conversion efficiency under 1-sun illumination, 100 mW/cm^2 (Fig. 11). The poor performance is likely due to a limited carrier collection length and a non-ideal band-alignment between CdS and SnSe. Follow-up studies are being conducted to improve performance. In particular, developing suitable buffer layers that form

Table 2
Electrical Properties of undoped and Sb/In doped SnSe thin films.

	Carrier density (/cm^3)	Mobility ($cm^2/V\cdot s$)	Resistivity ($\Omega\cdot cm$)	Conductivity (S/cm)
Undoped	1.03×10^{17}	1.27×10^{0}	4.82×10^{1}	2.09×10^{-2}
Sb doped	2.16×10^{15}	6.29×10^{-1}	4.59×10^{3}	2.18×10^{-4}
In doped	8.52×10^{14}	8.85×10^{0}	1.93×10^{3}	5.25×10^{-4}

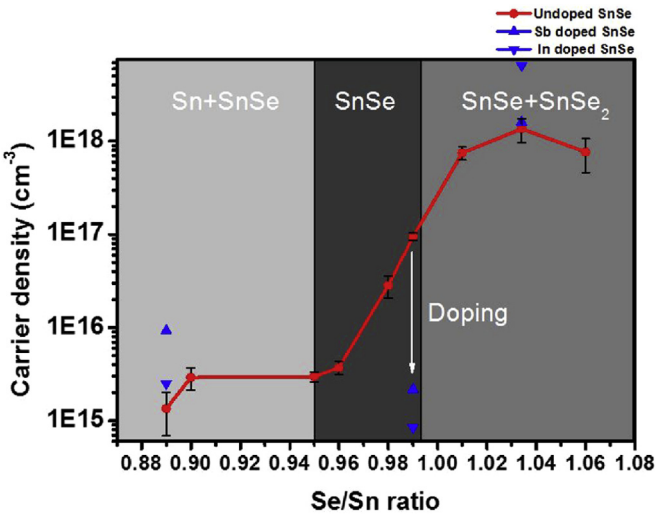

Fig. 9. Alteration of carrier concentration via stoichiometry control and counter doping.

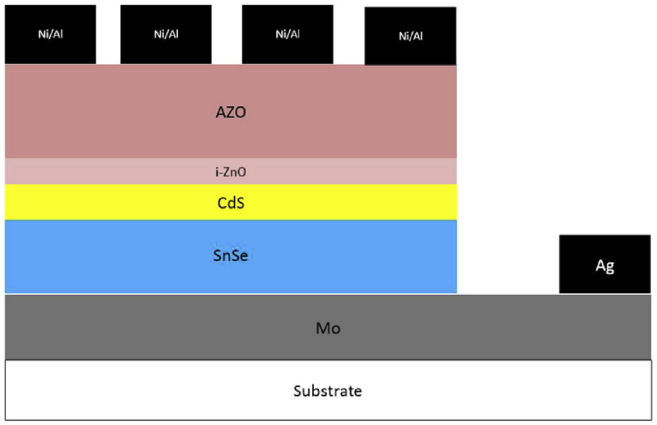

Fig. 10. Device structure of SnSe solar cell.

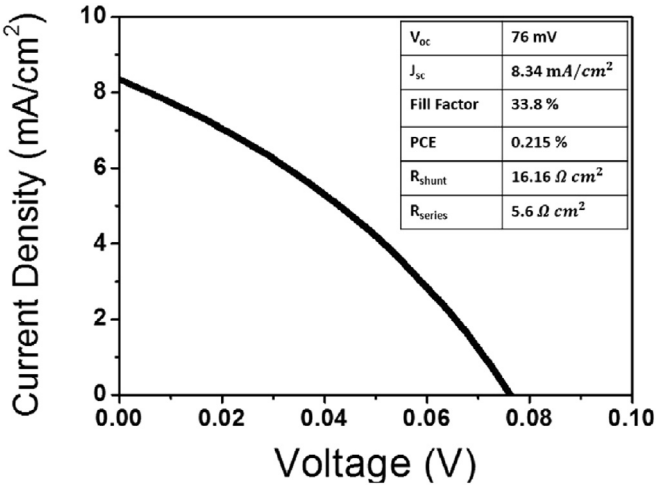

Fig. 11. Current-voltage curve under 1-Sun illumination from a solar cell with a SnSe absorber layer.

ideal band alignment with SnSe absorbers, the so-called "spike" type alignment, is priority [40].

4. Conclusions

In summary, we prepared single phase SnSe thin films using thermal co-evaporation with a thermal cracking source for selenium followed by post-deposition annealing process. It is shown that single-phase SnSe only exist in a narrow range of stoichiometry (Se/Sn = 0.95–0.99), which illustrates a difficulty in preparing single-phase SnSe films. By carefully controlling Sn and Se flux during deposition, we managed to achieve the target stoichiometry. Even in the single-phase range, electrical conductivity of SnSe is found to be very sensitive to the Se/Sn ratio; carrier concentration of samples varied over three orders of magnitude (10^{15} cm^{-3}–10^{17} cm^{-3}). Therefore, fine control of stoichiometry is very critical in device application of SnSe. Alternatively, our study suggests that SnSe can be adapted to a wide range of application due to its wide tenability of carrier concentration. For instance, SnSe films with a carrier density of ~10^{15} cm^{-3} would be suitable for photovoltaic devices and those with a higher carrier density for thermoelectric devices. In addition, we demonstrated that extrinsic doping of foreign elements such as Sn and In can be another method to further control carrier density of SnSe, although this approach is not very efficient given a small number (~10^{-4}) of the ionized fraction of the introduced dopants. A working SnSe photovoltaic device is demonstrated by using a slightly Sn-rich SnSe absorber, i.e., with carrier density of ~10^{15} cm^{-3}. We believe it is worthwhile to apply Se-rich SnSe, i.e., with a higher carrier density, to thermoelectric devices.

Acknowledgements

This work was supported by the National Research Foundation of Korea (NRF) [grant number 2015R1A2A2A04004945] and by the Technology Development Program to Solve Climate Changes of the National Research Foundation (NRF) funded by the Ministry of Science, ICT & Future Planning (No. 2016M1A2A2936757).

References

[1] P. Sinsermsuksakul, L. Sun, S.W. Lee, H.H. Park, S.B. Kim, C. Yang, R.G. Gordon, Overcoming efficiency limitations of SnS-based solar cells, Adv. Energy Mater. 4 (15) (2014) 1400496.
[2] Y. Zhou, L. Wang, S. Chen, S. Qin, X. Liu, J. Chen, D.-J. Xue, M. Luo, Y. Cao, Y. Cheng, E.H. Sargent, J. Tang, Thin-film Sb2Se3 photovoltaics with oriented one-dimensional ribbons and benign grain boundaries, Nat. Photonics 9 (6) (2015) 409–415.
[3] R. Indirajith, T.P. Srinivasan, K. Ramamurthi, R. Gopalakrishnan, Synthesis, deposition and characterization of tin selenide thin films by thermal evaporation technique, Curr. Appl. Phys. 10 (6) (2010) 1402–1406.
[4] V. Steinmann, R. Jaramillo, K. Hartman, R. Chakraborty, R.E. Brandt, J.R. Poindexter, Y.S. Lee, L. Sun, A. Polizzotti, H.H. Park, R.G. Gordon, T. Buonassisi, 3.88% efficient tin sulfide solar cells using congruent thermal evaporation, Adv. Mater. 26 (44) (2014) 7488–7492.
[5] P. Sinsermsuksakul, J. Heo, W. Noh, A.S. Hock, R.G. Gordon, Atomic layer deposition of tin monosulfide thin films, Adv. Energy Mater. 1 (6) (2011) 1116–1125.
[6] P.P. Hankare, A.V. Jadhav, P.A. Chate, K.C. Rathod, P.A. Chavan, S.A. Ingole, Synthesis and characterization of tin sulphide thin films grown by chemical bath deposition technique, J. Alloys Compd. 463 (1–2) (2008) 581–584.
[7] K. Hartman, J.L. Johnson, M.I. Bertoni, D. Recht, M.J. Aziz, M.A. Scarpulla, T. Buonassisi, SnS thin-films by RF sputtering at room temperature, Thin Solid Films 519 (21) (2011) 7421–7424.
[8] Y.C. Choi, D.U. Lee, J.H. Noh, E.K. Kim, S.I. Seok, Highly improved Sb2S3 sensitized-inorganic–organic heterojunction solar cells and quantification of traps by deep-level transient spectroscopy, Adv. Funct. Mater. 24 (23) (2014) 3587–3592.

[9] L.-D. Zhao, S.-H. Lo, Y. Zhang, H. Sun, G. Tan, C. Uher, C. Wolverton, V.P. Dravid, M.G. Kanatzidis, Ultralow thermal conductivity and high thermoelectric figure of merit in SnSe crystals, Nature 508 (7496) (2014) 373–377.
[10] A. Shafique, Y.-H. Shin, Thermoelectric and phonon transport properties of two-dimensional IV–VI compounds, Sci. Rep. 7 (1) (2017) 506.
[11] Y. Xiao, C. Chang, Y. Pei, D. Wu, K. Peng, X. Zhou, S. Gong, J. He, Y. Zhang, Z. Zeng, Origin of low thermal conductivity in SnSe, Phys. Rev. B 94 (12) (2016) 125203.
[12] L.-D. Zhao, G. Tan, S. Hao, J. He, Y. Pei, H. Chi, H. Wang, S. Gong, H. Xu, V.P. Dravid, C. Uher, G.J. Snyder, C. Wolverton, M.G. Kanatzidis, Ultrahigh power factor and thermoelectric performance in hole-doped single-crystal SnSe, Science 351 (6269) (2016) 141–144.
[13] A.T. Duong, G.D. Van Quang Nguyen, S.K. Van Thiet Duong, J.Y. Song, J.K. Lee, J.E. Lee, S. Park, T. Min, J. Lee, J. Kim, Achieving ZT= 2.2 with Bi-doped n-type SnSe single crystals, Nat. Commun. 7 (2016) 13713.
[14] B.G. Mendis, M.C.J. Goodman, J.D. Major, A.A. Taylor, K. Durose, D.P. Halliday, The role of secondary phase precipitation on grain boundary electrical activity in Cu2ZnSnS4 (CZTS) photovoltaic absorber layer material, J. Appl. Phys. 112 (12) (2012) 124508.
[15] Y. Feutelais, M. Majid, B. Legendre, S.G. Frics, Phase diagram investigation and proposition of a thermodynamic evaluation of the Tin-Selenium system, J. Phase Equilib. 17 (1) (1996) 40–49.
[16] N. Kumar, V. Sharma, N. Padha, N.M. Shah, M.S. Desai, C.J. Pancahl, I.Y. Protsenko, Influence of the substrate temperature on the structural, optical, and electrical properties of tin selenide thin films deposited by thermal evaporation method, Cryst. Res. Technol. 45 (1) (2010) 53–58.
[17] M. Sharon, K. Basavasawaran, Photoelectrochemical studies on p-SnSe electrodes, Sol. Cells 20 (4) (1987) 323–332.
[18] D.-H. Cho, W.-J. Lee, S.-W. Park, J.-H. Wi, W.S. Han, J. Kim, M.-H. Cho, D. Kim, Y.-D. Chung, Non-toxically enhanced sulfur reaction for formation of chalcogenide thin films using a thermal cracker, J. Mater. Chem. A 2 (35) (2014) 14593–14599.
[19] B. Shin, O. Gunawan, Y. Zhu, N.A. Bojarczuk, S.J. Chey, S. Guha, Thin film solar cell with 8.4% power conversion efficiency using an earth-abundant Cu2ZnSnS4 absorber, Prog. Photovolt. Res. Appl. 21 (1) (2013) 72–76.
[20] T.K. Todorov, K.B. Reuter, D.B. Mitzi, High-efficiency solar cell with earth-abundant liquid-processed absorber, Adv. Mater. 22 (20) (2010) E156–E159.
[21] J.J. Scragg, T. Ericson, T. Kubart, M. Edoff, C. Platzer-Björkman, Chemical insights into the instability of Cu2ZnSnS4 films during annealing, Chem. Mater. 23 (20) (2011) 4625–4633.
[22] H.R. Jung, S.W. Shin, K.V. Gurav, M.G. Gang, J.Y. Lee, J.H. Moon, J.H. Kim, Evolution of detrimental secondary phases in unstable Cu2ZnSnS4 films during annealing, Electron. Mater. Lett. 12 (1) (2016) 139–146.
[23] J. Xu, Y. Liu, Y. Yang, Fabrication of Cu2Zn(Sn,Si)S4 thin films using a two-step method for solar cell applications, Electron. Mater. Lett. 12 (6) (2016) 761–767.
[24] H. Song, S.-Y. Son, S.K. Kim, G.Y. Jung, A facile synthesis of hierarchical Sn3O4 nanostructures in an acidic aqueous solution and their strong visible-light-driven photocatalytic activity, Nano Res. 8 (11) (2015) 3553–3561.
[25] P.A. Fernandes, M.G. Sousa, P.M.P. Salome, J.P. Leitao, A.F. da Cunha, Thermodynamic pathway for the formation of SnSe and SnSe2 polycrystalline thin films by selenization of metal precursors, Cryst. Eng. Comm. 15 (47) (2013) 10278–10286.
[26] H.R. Chandrasekhar, R.G. Humphreys, U. Zwick, M. Cardona, Infrared and Raman spectra of the IV-VI compounds SnS and SnSe, Phys. Rev. B 15 (4) (1977) 2177–2183.
[27] K. Tanaka, N. Moritake, H. Uchiki, Preparation of thin films by sulfurizing sol–gel deposited precursors, Sol. Energy Mat. Sol. C 91 (13) (2007) 1199–1201.
[28] A. Tanuševski, D. Poelman, Optical and photoconductive properties of SnS thin films prepared by electron beam evaporation, Sol. Energy Mater. Sol. C 80 (3) (2003) 297–303.
[29] L. Makinistian, E.A. Albanesi, On the band gap location and core spectra of orthorhombic IV–VI compounds SnS and SnSe, Phys. Status Solidi (B) 246 (1) (2009) 183–191.
[30] N.R. Mathews, Electrodeposited tin selenide thin films for photovoltaic applications, Sol. Energy 86 (4) (2012) 1010–1016.
[31] T.Q. Dang, SnSe thin films synthesized by solid state reactions, Thin Solid Films 149 (2) (1987) 197–203.
[32] K.J. John, B. Pradeep, E. Mathai, Tin selenide (SnSe) thin films prepared by reactive evaporation, J. Mater. Sci. 29 (6) (1994) 1581–1583.
[33] R.H. Bube, Electrons in Solids: an Introductory Survey, Academic Press, 1992.
[34] G. Shi, E. Kioupakis, Quasiparticle band structures and thermoelectric transport properties of p-type SnSe, J. Appl. Phys. 117 (6) (2015) 065103.
[35] J.T. Heath, J.D. Cohen, W.N. Shafarman, Bulk and metastable defects in CuIn1−xGaxSe2 thin films using drive-level capacitance profiling, J. Appl. Phys. 95 (3) (2004) 1000–1010.
[36] H. Şafak, M. Merdan, Ö.F. Yüksel, Dispersion analysis of SnS and SnSe, Turk. J. Phys. 26 (5) (2002) 341–348.
[37] Y. Kumagai, L.A. Burton, A. Walsh, F. Oba, Electronic structure and defect physics of tin sulfides: SnS, Sn 2 S 3, and Sn S 2, Phys. Rev. Appl. 6 (1) (2016) 014009.
[38] J. Vidal, S. Lany, M. d'Avezac, A. Zunger, A. Zakutayev, J. Francis, J. Tate, Band-structure, optical properties, and defect physics of the photovoltaic semiconductor SnS, Appl. Phys. Lett. 100 (3) (2012) 032104.
[39] P. Sinsermsuksakul, R. Chakraborty, S.B. Kim, S.M. Heald, T. Buonassisi, R.G. Gordon, Antimony-doped tin(II) sulfide thin films, Chem. Mater. 24 (23) (2012) 4556–4562.
[40] T. Minemoto, Y. Hashimoto, T. Satoh, T. Negami, H. Takakura, Y. Hamakawa, Cu (In, Ga) Se 2 solar cells with controlled conduction band offset of window/Cu (In, Ga) Se 2 layers, J. Appl. Phys. 89 (12) (2001) 8327–8330.